Characterization of the structure–function relationship at the ligament-to-bone interface

Kristen L. Moffat*, Wan-Hsuan S. Sun*, Paul E. Pena*, Nadeen O. Chahine†, Stephen B. Doty‡, Gerard A. Ateshian†, Clark T. Hung§, and Helen H. Lu*¶‖

*Biomaterials and Interface Tissue Engineering Laboratory, Department of Biomedical Engineering, Columbia University, New York, NY 10027; †Musculoskeletal Biomechanics Laboratory, Departments of Biomedical and Mechanical Engineering, Columbia University, New York, NY 10027; ‡Analytical Microscopy Laboratory, Hospital for Special Surgery, New York, NY 10021; §Cellular Engineering Laboratory, Department of Biomedical Engineering, Columbia University, New York, NY 10027; and ¶College of Dental Medicine, Columbia University, New York, NY 10032

Edited by Robert Langer, Massachusetts Institute of Technology, Cambridge, MA, and approved April 11, 2008 (received for review December 28, 2007)

Soft tissues such as ligaments and tendons integrate with bone through a fibrocartilaginous interface divided into noncalcified and calcified regions. This junction between distinct tissue types is frequently injured and not reestablished after surgical repair. Its regeneration is also limited by a lack of understanding of the structure–function relationship inherent at this complex interface. Therefore, focusing on the insertion site between the anterior cruciate ligament (ACL) and bone, the objectives of this study are: (*i*) to determine interface compressive mechanical properties, (*ii*) to characterize interface mineral presence and distribution, and (*iii*) to evaluate insertion site-dependent changes in mechanical properties and matrix mineral content. Interface mechanical properties were determined by coupling microcompression with optimized digital image correlation analysis, whereas mineral presence and distribution were characterized by energy dispersive x-ray analysis and backscattered scanning electron microscopy. Both region- and insertion-dependent changes in mechanical properties were found, with the calcified interface region exhibiting significantly greater compressive mechanical properties than the noncalcified region. Mineral presence was only detectable within the calcified interface and bone regions, and its distribution corresponds to region-dependent mechanical inhomogeneity. Additionally, the compressive mechanical properties of the tibial insertion were greater than those of the femoral. The interface structure–function relationship elucidated in this study provides critical insight for interface regeneration and the formation of complex tissue systems.

anterior cruciate ligament | calcium phosphate | fibrocartilage | insertion site | compression

Functional integration between soft and hard tissues is essential for musculoskeletal motion. Many soft tissues, such as the anterior cruciate ligament (ACL), insert into subchondral bone through a multitissue interface, which enables the soft and hard tissues to function in unison, and in turn facilitates physiological loading and joint motion. The ACL is the major intra-articular ligament of the knee, and it connects the femur and tibia through two insertion sites with characteristic spatial variations in cell type and matrix composition (1–8). It has long been postulated that controlled matrix heterogeneity inherent at the ligament-to-bone interface serves to minimize the formation of stress concentrations, and to enable the transfer of complex loads between soft tissue and bone (2, 9). The insertion site is prone to injury, however, and mechanical fixation of current reconstruction grafts fails to preserve or reestablish the anatomic ligament-to-bone enthesis. Absence of this critical interface compromises graft stability and long-term clinical outcome (10–13); thus, its regeneration will be essential for functional graft-to-bone integration and ultimately biological graft fixation.

A critical step in any regeneration or tissue engineering effort is the determination of the material properties of the tissue to be replaced. Similarly for the soft tissue-to-bone interface, developing an understanding of its structure–function relationship is a prerequisite for interface regeneration. It has been reported that direct ligament-to-bone insertion sites are anatomically divided into four distinct yet continuous tissue regions, with region-specific cell type and matrix composition (1–8). The first region is the ligament proper that contains fibroblasts within a matrix rich in collagens I and III. Directly adjacent to the ligament is the fibrocartilage interface that is further divided into noncalcified and calcified regions. The nonmineralized fibrocartilage (NFC) is composed of fibrochondrocytes in a matrix of collagens I and II, whereas hypertrophic chondrocytes within a collagen X matrix are found in the mineralized fibrocartilage (MFC) region. The MFC then connects directly to subchondral bone. This region-dependent matrix heterogeneity is postulated to permit a gradual increase in stiffness across the interface regions, thereby minimizing stress concentrations and allowing for effective load transfer from ligament to bone (14, 15). Partition of the fibrocartilage interface into nonmineralized and mineralized regions is anticipated to have a functional significance, as increases in matrix mineral content have been associated with higher mechanical properties in connective tissues (16–18).

Although the biochemical composition of the ACL-to-bone insertion has been characterized, its mechanical properties are not known. Thus, the structure–function relationship at this critical junction is poorly understood. The interface has been understudied, because experimental determination of insertion site properties by classical mechanical testing methods is particularly challenging, largely due to the structural complexity and relatively small scale of the interface, which averages from 100 μm to 1 mm in length depending on species and age (1, 8, 14). Current knowledge of interface mechanical properties has thus been derived largely from theoretical predictions (15). Finite-element analysis of the medial collateral ligament (MCL) loaded in tension predicted that the largest principal tensile stresses are located within the ligament midsubstance, whereas the greatest principal *compressive* stresses occur near the distal edge of the MCL-to-bone insertion (15). Additionally, several early studies have reported that insertion site deformation can vary significantly from that of the ligament substance (9, 14, 19, 20). Taken collectively, these results suggest that interface matrix organization and composition allow for a mechanical response which differs from that of the soft tissue or bone.

Author contributions: K.L.M. and H.H.L. designed research; K.L.M. performed research; K.L.M., N.O.C., S.B.D., G.A.A., C.T.H., and H.H.L. contributed new reagents/analytic tools; K.L.M., W.-H.S.S., P.E.P., N.O.C., S.B.D., G.A.A., C.T.H., and H.H.L. analyzed data; and K.L.M. and H.H.L. wrote the paper.

The authors declare no conflict of interest.

This article is a PNAS Direct Submission.

‖To whom correspondence should be addressed. E-mail: hl2052@columbia.edu.

This article contains supporting information online at www.pnas.org/cgi/content/full/0712150105/DCSupplemental.

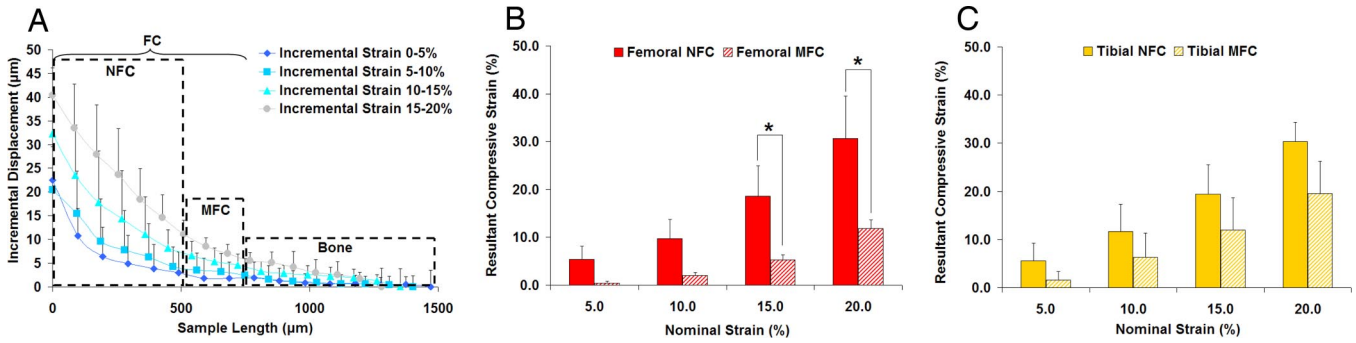

Fig. 1. Region-dependent strain response under uniaxial unconfined compression. (*A*) Representative displacement profile of the insertion site under microcompression. Nonlinear displacement was found, decreasing in magnitude from nonmineralized (NFC) to mineralized fibrocartilage (MFC) and to bone. Axial compressive strain for the femoral (*B*) and tibial insertion regions (*C*). The strain experienced by the NFC is consistently higher than the MFC, and this difference was significant for the femoral insertion at 15% and 20% strain (*, $P < 0.05$).

To circumvent the experimental challenges associated with interface characterization by conventional methods, we recently used ultrasound elastography to map the displacement and strain distribution at the ACL-to-bone interface (21). Elastography analyses revealed that displacement under applied tension across the insertion is region-dependent, with the highest deformation found within the ACL, then decreasing in magnitude from the interface to bone. In addition, both tensile and compressive strains were detected at the insertion site. Building on these promising results, the goal of this study is to determine the compressive mechanical properties of the ACL-to-bone interface and to characterize region-dependent changes across the insertion site. Moreover, to elucidate the interface structure–function relationship and decipher the contribution of specific matrix constituents to any observed changes in mechanical properties, the mineral presence and distribution across the interface regions will be evaluated. To determine interface mechanical properties, uniaxial microcompression testing is combined with video-microscopy and optimized Digital Image Correlation (DIC) analysis (22–24). This method has been used to evaluate the mechanical anisotropy of articular cartilage, and two-dimensional deformation fields are determined with high accuracy (22, 23). By tracking the location and displacement of texture patterns, optimized DIC can directly deduce surface deformation with subpixel accuracy (23). It is particularly useful for interface characterization, because relatively small tissue regions can be evaluated at significantly higher resolutions than conventional methods with traditional surface markers.

Therefore, by using functional imaging as well as classical material characterization methods, this study has three objectives: (*i*) to determine the compressive mechanical properties of the nonmineralized and mineralized region of the fibrocartilage interface, (*ii*) to characterize the mineral presence and distribution at the interface, and (*iii*) to compare the mechanical properties and matrix content of the tibial and femoral insertion sites. Displacement, stress–strain profiles, and Young's moduli of the interface regions will be determined under uniaxial unconfined compression. Additionally, backscattered scanning electron microscopy (bSEM) combined with energy dispersive x-ray analysis (EDAX) will be used to determine the elemental composition of the fibrocartilage interface. Both region- and insertion-dependent changes in compressive mechanical properties and matrix mineral content are anticipated. It is expected that findings of this study will provide insight into interface structure–function relationship, as well as identify the critical biomimetic design parameters for interface regeneration and the formation of integrated tissue systems.

Results

Region-Dependent Interface Mechanical Properties. Significant changes in mechanical properties were observed across the different regions of the ACL-to-bone insertion. As shown in Fig. 1*A*, uniaxial unconfined compression resulted in nonlinear axial deformation across the interface, specifically from the nonmineralized fibrocartilage (NFC) to the mineralized fibrocartilage (MFC), and then to the bone region. Additionally, the NFC exhibited greater deformation than the MFC region at all applied strains. At 5% and 10% nominal strain, deformation occurred mostly in the NFC. When the applied nominal strain was increased to 15% and 20%, deformation became more evident in the MFC. It is noted that within each of the interface regions, the deformation was nearly linear, especially at 10% strain or higher [supporting information (SI) Table S1], indicating good contact between the sample and platens.

To represent the true strain experienced by the tissue regions, the DIC resultant strain instead of the nominal strain is plotted in Figs. 1–3. Similar to the displacement profile, the resultant strain at the interface was also region-dependent. As seen in Fig. 1 *B* and *C*, the NFC experienced greater resultant strain than the MFC region for both the femoral and tibial samples at all applied nominal strains. When 10% nominal strain was applied to the femoral insertion, the NFC deformed by 9.7% whereas the resultant strain found in the MFC region was only 2.0%. A similar region-dependent strain profile was observed for the tibial insertion, with the resultant DIC strain decreasing from 12.8% to 6.3% progressing from the NFC to MFC region, and averaging 25.7% across the entire fibrocartilage interface.

To determine the equilibrium mechanical properties of the interface regions, the resultant compressive strains were plotted against the corresponding measured stresses and interpolated by using a Matlab cubic spline algorithm. As shown in Fig. 2, the axial stress was significantly greater for the MFC than for the NFC region at 10% strain, regardless of the insertion site from which the sample originated. Furthermore, apparent Young's modulus (E_Y) was found to be significantly greater for the calcified than for the noncalcified interface region (Fig. 2 *C* and *D*). Specifically, the modulus for the femoral MFC was 87% greater at 5% strain and 66% greater at 10% strain than the femoral NFC at the respective resultant strains. Similarly, compared with the tibial NFC, the modulus for the tibial MFC was determined to be 76% greater at 5% strain, and 43% greater at 10% strain.

Insertion Site-Dependent Mechanical Properties. Differences in the tibial and femoral insertion mechanical properties were also found in this study. Initial analysis of the mechanical properties of the full-thickness fibrocartilage (FC) region revealed that axial stress did not vary significantly between the femoral and tibial insertion sites (data not shown). However, further analysis revealed that the stresses observed at both the NFC (Fig. 3*A*) and MFC (Fig. 3*B*) interface regions were consistently greater for the tibial than the

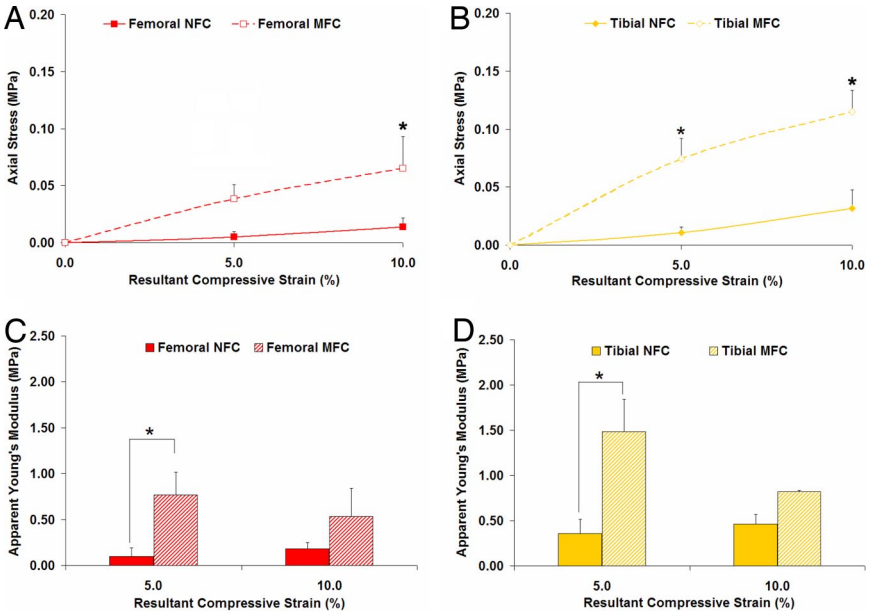

Fig. 2. Region-dependent mechanical properties at the insertion site. Equilibrium axial stress ($n = 3$) (*A* and *B*) and apparent Young's modulus ($n = 3$) (*C* and *D*) of the nonmineralized (NFC) and mineralized fibrocartilage (MFC) regions at 5% and 10% resultant strain. Note the significantly higher axial stress as well as the significantly greater apparent Young's modulus found for the MFC region (*, $P < 0.05$).

femoral insertion site, with a significantly higher axial stress found for the tibial MFC at 10% resultant strain ($P < 0.05$).

Additionally, insertion-dependent differences in apparent Young's modulus (E_Y) were observed (Fig. 3*C*). Although no significant change in E_Y was found for the femoral and tibial full-thickness fibrocartilage (data not shown), further analysis of E_Y for the NFC and MFC regions revealed that the tibial NFC and MFC regions exhibited a greater E_Y, on average, when compared with their femoral counterparts at both 5% and 10% resultant compressive strain. It was found that at 5% strain, the equilibrium modulus of the tibial NFC region was 73% greater than that of the femoral NFC. Similarly, the E_Y of the tibial MFC was consistently greater than the femoral MFC at 5% and 10% applied strain (Fig. 3*C*).

Region-Dependent Mineral Presence and Distribution. The bright areas in the bSEM image correspond to elements with higher atomic number, such as calcium (Ca) and phosphorous (P). Mineral presence was detected only in the MFC and bone regions. As seen in Fig. 4, the MFC region is a relatively thin area composed of a densely mineralized matrix, whereas the bone region consists of a mineralized porous matrix. The junction between the NFC and MFC was characterized by "fingers" of mineralized matrix surrounding the hypertrophic chondrocyte lacunae. As confirmed by von Kossa (Fig. 4*A*), backscattered images of the insertion (Fig. 4*B*) revealed a sharp transition in mineral content between the NFC and MFC.

Calcium phosphate presence and region-dependent changes across the interface were also characterized by energy dispersive x-ray analysis (EDAX). The representative elemental composition profiles at each interface region of the tibial and femoral insertion sites are shown in Fig. 4*C* (Ca, P, S; see arrows). The Ca and P peaks associated with mineral presence were only detectable in the MFC and bone regions. As expected, the highest peak intensities for Ca and P were found in the bone region, and diminished thereafter in the MFC region. Additionally, sulfur (S), which is likely associated with sulfated proteoglycans and protein presence, was detected in all interface regions examined (Fig. 4*C*). The highest S peak intensity was found in the NFC region, and it decreased thereafter from the MFC to the bone region. Mineral distribution across the insertion was further characterized with EDAX line scan analysis. As shown in Fig. 5, Ca and P were only present in the MFC and bone regions, and more importantly, corresponding Ca and P elemental profiles were observed within each of the mineral containing regions.

Insertion Site-Dependent Matrix Composition. At both insertion sites, mineral presence was only detected in the MFC and bone regions (Fig. 5), with no observable difference in mineral distribution found between these interfaces.

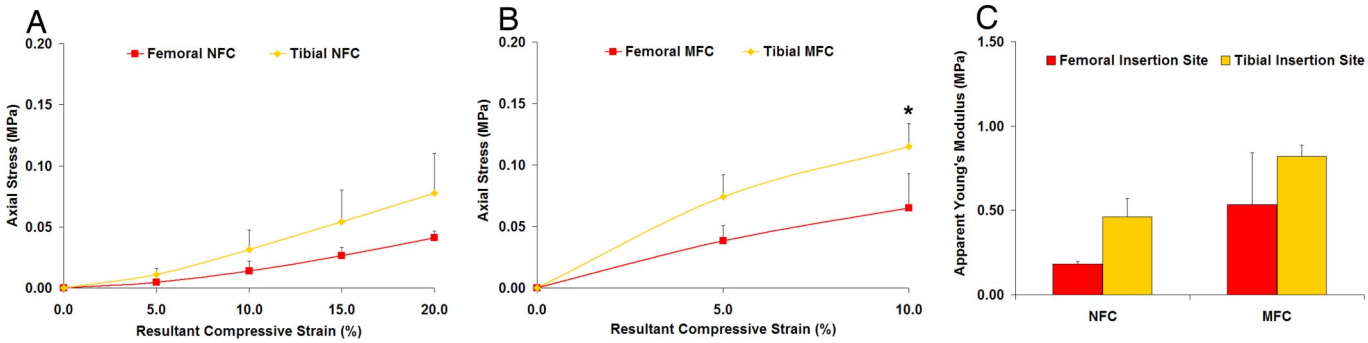

Fig. 3. Insertion site-dependent mechanical heterogeneity. Equilibrium axial stress of nonmineralized (NFC) (*A*) and mineralized fibrocartilage (MFC) (*B*) regions ($n = 3$; *, $P < 0.05$). Significantly higher axial stress was found for the tibial compared with the femoral insertion at 10% resultant strain. (*C*) Incremental apparent Young's modulus ($n = 3$) of the femoral and tibial NFC and MFC regions at 10% resultant compressive strain.

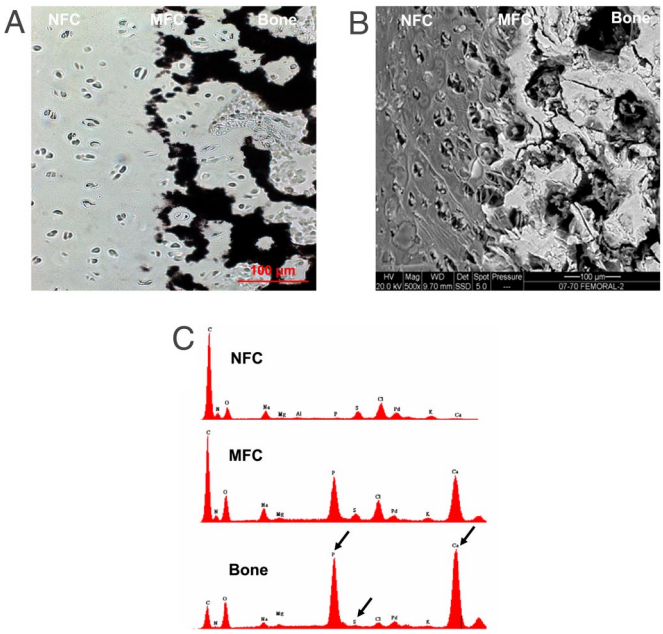

Fig. 4. Mineral presence and distribution at the ACL-to-bone insertion. (*A*) von Kossa (20×) (Scale bar, 100 μm.) (*B*) Backscattered SEM micrographs (500×) for the femoral insertion site. (Scale bar, 100 μm.) Note that mineral presence is only detectable in the mineralized fibrocartilage (MFC) and bone regions. (*C*) Representative EDAX spectra of nonmineralized fibrocartilage (NFC), mineralized fibrocartilage (MFC), and bone regions of the femoral insertion. The calcium (Ca) and phosphorous (P) peaks (arrows) are only detectable in MFC and bone.

Discussion

The objectives of this study are to characterize the compressive mechanical properties as well as mineral distribution at the tibial and femoral ACL-to-bone insertion sites. Both region-dependent mechanical inhomogeneity and mineral distribution are observed at the interface. Calcium phosphate presence is only detectable within the mineralized fibrocartilage and bone regions, and a sharp transition, instead of a gradient of mineral distribution, is observed progressing from the nonmineralized to the mineralized interface regions. Furthermore, the interface regions of the tibial insertion site exhibit greater compressive mechanical properties compared to their femoral counterparts.

The region-dependent mechanical properties observed at the ACL-to-bone interface are highly significant when considering the functionality of the insertion site. Under applied compression, a gradual decrease in insertion site strain is found progressing from the nonmineralized fibrocartilage to mineralized fibrocartilage, and then to the bone region, accompanied by a corresponding increase in apparent Young's modulus across the interface. This mechanical inhomogeneity serves to minimize the formation of stress concentrations and promote gradual load transfer from the soft (i.e., ligament) to hard (i.e., bone) tissue. A similar mechanical response has been reported for other stratified connective tissues such as articular cartilage (22–25) and growth plate cartilage (18), which also exhibit region-dependent inhomogeneity. Schinagl *et al.* (24) isolated osteochondral constructs from adult bovine knee, and found that under uniaxial confined compression, the strain decreased from the articular surface to the subchondral bone. The equilibrium aggregate modulus of the deep layer was also significantly higher than that of the superficial cartilage layer. By using unconfined compression and optimized DIC analysis, Wang *et al.* (23) evaluated depth-dependent inhomogeneity of articular cartilage from carpometacarpal joints of immature calves, and reported a higher equilibrium modulus for the deep layer compared with the superficial cartilage layers.

The apparent Young's modulus of the insertion fibrocartilage reported in the present study is similar in magnitude to that of articular cartilage tested under similar conditions (23). Wang *et al.* (8) reported an equilibrium modulus of 0.23 ± 0.10 MPa for the superficial layer and 1.51 ± 0.72 MPa for the deep layer of articular cartilage. The Young's moduli of the nonmineralized and mineralized fibrocartilage regions are within range of those of articular cartilage. Similarity between the insertion fibrocartilage and articular cartilage may not be surprising, especially in immature animal models. Wang *et al.* (8) conducted an age-dependent characterization of the biochemical composition of the ACL-to-bone insertion, and reported that the morphology, collagen type, and proteoglycan distribution of the immature bovine fibrocartilage insertion resembled that of the hyaline cartilage of the same age. As the interface matures, however, penetration of the fibrocartilage matrix with nonmineralized and mineralized collagen fibers is expected to alter the mechanical response of the interface regions. These age-dependent changes in structural organization are likely in response to postnatal physiological loading, and their effect on the insertion mechanical properties will be examined in future studies.

Both region-dependent changes in mechanical properties and mineral distribution are observed in this study, which suggests an inherent structure–function relationship at the ACL-to-bone interface. Similarly, the mechanical response of hyaline cartilage has been related to matrix mineral content in both mineralized and osteoarthritic cartilage (16–18). Ferguson *et al.* (17) reported a positive correlation between indentation modulus and hardness with mineral content in calcified articular cartilage. In this study, the observed increase in compressive modulus and axial stress from the nonmineralized to mineralized fibrocartilage is likely associated with the onset of mineral presence in the calcified fibrocartilage region (Fig. 6). Linear regression analysis revealed a strongly positive correlation between material properties and mineral content, with a correlation coefficient (R) of 0.8835 for Young's modulus vs. calcium intensity, and an R value of 0.8677 for modulus vs. phosphorous peak intensity. In the absence of mineral, increases in proteoglycan and matrix water content have been associated with higher equilibrium modulus from the surface to the deep layer of

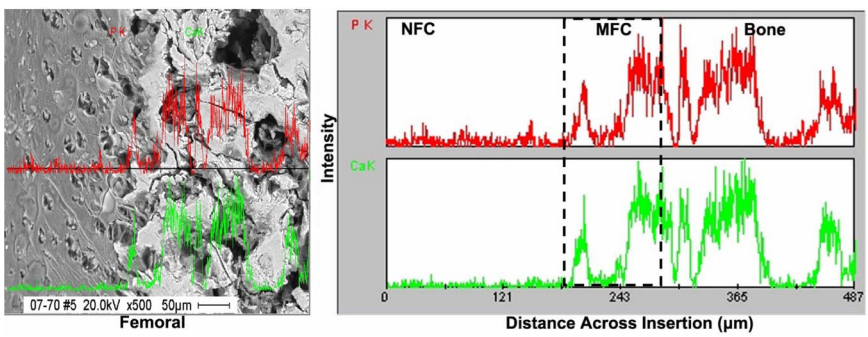

Fig. 5. Distribution of calcium (Ca) and phosphorous (P) across the insertion. EDAX line scan analysis of the femoral insertion (red, phosphorous; green, calcium; 500×). Calcium and phosphorous peaks are only identified within the mineralized fibrocartilage (MFC) and bone regions, with corresponding Ca–P profiles, which signifies the presence of calcium phosphate.

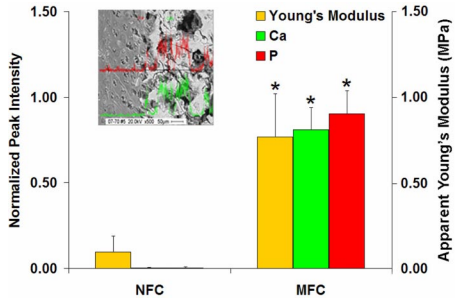

Fig. 6. Structure–function relationship at the ACL-to-bone insertion. Progressing from the nonmineralized fibrocartilage (NFC) region to the mineralized fibrocartilage (MFC) region, an abrupt and significant increase in mineral (Ca and P) is observed that corresponds to a significant increase in incremental apparent Young's modulus (*, $P < 0.05$; femoral insertion).

articular cartilage (24). Elemental analysis of the interface regions reveals an increase in sulfur peak intensity as calcium and phosphorous peak intensities decreased, suggesting a diminishing role for proteoglycans in the mineralized fibrocartilage region. Therefore, the region-dependent changes in compressive mechanical properties observed in this study may be attributed to mineral presence and distribution at the mineralized fibrocartilage region. It is likely that through particulate strengthening, the mineral phase can decrease deformation and augment matrix stiffness across the interface regions.

In addition to region-dependent variations in tissue mechanical properties and matrix composition, differences in mechanical properties are identified between the tibial and femoral insertion sites. The apparent Young's modulus of the tibial insertion site is significantly higher than that of the femoral insertion, and this trend is consistently observed for the two interface fibrocartilage (NFC and MFC) regions. Site-dependent variations in mechanical properties within the knee joint have also been reported for articular cartilage (26, 27). Treppo *et al.* (27) found that the equilibrium modulus of cartilage was significantly higher for the anterior femoral condyle when compared with the anterior tibial plateau, and this difference was attributed to changes in proteoglycan content between the two regions. Because no difference in mineral distribution is detected between the tibial and femoral insertion sites, other matrix constituents may be responsible for the observed site-dependent differences in the current study. However, when total sulfated proteoglycan and collagen content between the two insertion sites were compared, no significant difference was observed (data not shown).

Based on these observations, it is likely that factors other than matrix content, that is, matrix distribution or organization, may be responsible for the difference between tibial and femoral ACL insertion site mechanical properties. Thomopoulos *et al.* (28) reported that collagen fiber orientation at the supraspinatus tendon-to-bone insertion may be related to variations in region-dependent mechanical properties. Additionally, Wang *et al.* (8) found that, although the femoral and tibial ligament-to-bone insertion sites were histologically similar, the organization of collagen fibers differed between these two interfaces. In this study, similar observations were made when collagen distribution at the two insertion sites was compared (data not shown). Specifically, although no significant difference was found in the angle of fiber insertion, collagen fibers penetrated deeper into the fibrocartilage region and appeared to assume greater organization at the tibial insertion. This apparent difference in collagen fiber organization may contribute to the insertion site-dependent changes identified in this study.

In addition to augmenting the current understanding of the soft tissue-to-bone insertion, elucidating the interface structure–function relationship is important for identifying biomimetic design parameters for interface regeneration. Furthermore, these values will serve as benchmark criteria for judging the success of the interface tissue engineering effort. Based on the findings of this study, it is anticipated that interface regeneration will require a multiphased scaffold that supports the establishment of distinct yet continuous tissue regions observed at the native interface (29, 30). Moreover, it will be critical to recapitulate, in stratified scaffold design, the aforementioned region-dependent changes in interface mechanical properties. In this study, the observed increase in elastic modulus progressing from the noncalcified to the calcified fibrocartilage region is attributed to the introduction of a calcium phosphate phase in the mineralized region. Therefore, from a biomimetic standpoint, one strategy for engineering controlled mechanical inhomogeneity on the interface scaffold is to exercise spatial control over the distribution and concentration of calcium phosphate on each scaffold phase.

The findings of this study also have broad appeal in efforts to engineer complex tissues or organ systems (31). The field of tissue engineering has in the past largely focused on formulating and validating a consistent experimental methodology for *ex vivo* regeneration of tissues such as bone, ligament, or tendon. Building on these successes and to enable clinical translation of tissue engineered grafts, the emphasis has now shifted from tissue formation to tissue function (32). A significant challenge in functional tissue engineering resides in how to integrate tissue engineered grafts with each other as well as with the host environment. With its focus on bridging distinct tissue types, interface tissue engineering would thus be instrumental for *ex vivo* development and *in vivo* translation of integrated musculoskeletal tissue systems with biomimetic complexity and functionality.

Future studies will focus on further elucidating interface structure–function relationships, by extending the current analysis to both adult and diseased models. This study used the immature model as ACL injuries occur largely in patients ranging from 15 to 25 years of age (33, 34), many of whom are still skeletally immature. Additionally, the compressive mechanical properties of the interface are evaluated here as fibrocartilaginous tissues are found largely in regions subjected to compression. Future work will extend the analysis of insertion site structure–function relationships to evaluation of the tensile and shear properties of the interface. These material properties can be determined by building on our ultrasound elastography analysis of the interface (21) as well as by using other functional imaging modalities such as magnetic resonance elastography (MRE) (35–38).

In summary, a multidisciplinary approach combining classical material characterization as well as state-of-the-art functional imaging methods was used in this study to evaluate the structure–function relationship of the ligament-to-bone interface. Both region- and insertion-dependent mechanical responses are observed across the insertion site. Moreover, regional matrix heterogeneity corresponds to greater compressive stress and equilibrium modulus at the calcified interface region. The increase in compressive mechanical properties from the noncalcified to the calcified fibrocartilage regions is attributed to mineral presence in the mineralized fibrocartilage region. These findings provide new insight into the structure–function relationship at this critical interface, and are highly significant for the regeneration of the soft tissue-to-bone interface and the future development of complex tissues or organ systems.

Materials and Methods

Sample Isolation. Insertion samples were isolated from immature bovine tibiofemoral joints ($n = 3$) obtained from a local abattoir. In brief, the patellar tendon was removed after the retraction of skin and s.c. fascia, and an incision was made into the joint capsule to expose the femoral condyle and tibial plateau. Both the femoral and tibial insertions were then identified and excised. Transverse cuts at 7 mm apart were made through the insertion samples, thereby

isolating rectangular specimens (Fig. S1*A*) containing regions of ligament (L), fibrocartilage (FC), and bone (B). All samples were stored at −20°C in PBS (PBS, Sigma-Aldrich). Before testing, the samples were cryo-sectioned (Leitz), and the length of each specimen (Table S2) was determined optically by using a calibrated 4× objective with a resolution of 1.66 μm per pixel. Sample width and height were measured and its cross-sectional area was calculated.

Microcompression Mechanical Testing. The samples were tested in uniaxial unconfined compression by using a custom loading device (22). To enhance surface texture, the samples were stained with a nuclear dye (Hoechst 33258, 10 μl/ml, Sigma-Aldrich; Fig. S1*B*). For microcompression, the sample immersed in PBS was positioned between two impermeable platens. The device was aligned on the motorized stage of an Olympus IX80 microscope, with the platens perpendicular to the moving axis of the stage. Uniaxial unconfined compression was applied by using a micrometer (1-μm resolution; MRO Industrial Supplies), and the equilibrium load was recorded by a load transducer (250 g, Sensotec). After the initial nominal 10% tare strain, which defined the reference configuration, additional uniaxial strain was applied at 5% increments at 1 μm/s relative to the unloaded sample length. The specimen was allowed to relax for 15 min before applying the next 5% strain increment. At equilibrium, an image of the sample with enhanced texture was acquired with a digital camera and the load was recorded. Deformation was incrementally applied until the sample had been compressed by 20%.

Region-Dependent Mechanical Properties. Incremental strain analysis was performed across the sample by using an optimized DIC algorithm (22, 23). In brief, after epifluorescence microscopy was used to image cell nuclei in the sample (Fig. 7*B*), DIC analysis, which optimally matches the texture of small regions of interest between the pre- and postcompression images, was performed. Comparison between these images allowed for quantification of the displacement field, and resultant strains were then determined from the spatial gradient of this displacement field within the two fibrocartilage interface regions (Table 1). The equilibrium normal stress was calculated based on the measured load and original cross-sectional area. A cubic spline Matlab interpolation algorithm was applied to the resultant axial strain and equilibrium stress data to evaluate stress at increments of 5% strain, referred to here as the resultant compressive strain and axial stress. The apparent incremental Young's modulus (E_Y) was determined from the slope of linear region of the axial stress vs. the resultant strain curve for the noncalcified and calcified interface regions.

Region-Dependent Mineral Presence and Distribution. Elemental composition and mineral distribution across the ACL-to-bone interface were determined by using scanning electron microscopy (SEM, FEI Quanta 600) coupled with energy dispersive x-ray analysis (EDAX, Phoenix Pro). In brief, the insertion samples (n = 3) were first fixed in 100% ethyl alcohol for 24 h, after which transverse cuts were made to obtain samples containing regions of ligament, fibrocartilage, and bone. After sputter-coating with palladium, the samples were imaged in both secondary and backscattered modes. In addition, EDAX was performed at 20 kV, and spectra were collected at the ligament, nonmineralized fibrocartilage (NFC), mineralized fibrocartilage (MFC), and bone regions. Points of analysis (n = 3 per region) were randomly chosen within each interface region. After background subtraction by a system standard, Ca and P peak intensity at the NFC and MFC regions were normalized to the corresponding peaks for bone. Line scan analysis was performed to characterize elemental distribution across the interface with EDAX spectra collected at 0.25-μm increments, yielding ≈490 data points for each sample (n = 3). Mineral distribution at the insertion (n = 2) was also assessed by von Kossa stain following published methods (8).

Statistical Analysis. Results are presented in mean ± standard deviation, with n = number of samples. A two-way ANOVA was performed, followed by a Tukey HSD *post hoc* test for all pairwise comparisons, and significance was attained at $P < 0.05$. The effect of percent strain, tissue region (NFC, MFC), or insertion site (tibial, femoral) on axial stress and Young's modulus were determined. Additionally, regression analysis of the correlation between apparent Young's modulus and peak intensities for Ca and P were determined across the interface regions (NFC and MFC). Statistical analyses were performed with JMPIN (4.0.4, SAS Institute).

ACKNOWLEDGMENTS. We thank Anthony Labissiere at the Hospital for Special Surgery for assistance with SEM/EDAX analysis, and Jeffrey Spalazzi at Columbia University for providing samples for von Kossa staining. This work was supported by National Institutes of Health-National Institute of Arthritis and Musculoskeletal and Skin Diseases Grant AR0524202-02 (to H.H.L.) and National Science Foundation Graduate Fellowship GK-12 0338329 (to K.L.M.).

1. Cooper RR, Misol S (1970) Tendon and ligament insertion: A light and electron microscopic study. *J Bone Joint Surg Am* 52:1–20.
2. Benjamin M, Evans EJ, Copp L (1986) The histology of tendon attachments to bone in man. *J Anat* 149:89–100.
3. Niyibizi C, Visconti CS, Kavalkovich K, Woo SL (1995) Collagens in an adult bovine medial collateral ligament: Immunofluorescence localization by confocal microscopy reveals that type XIV collagen predominates at the ligament-bone junction. *Matrix Biol* 14:743–751.
4. Niyibizi C, Sagarrigo VC, Gibson G, Kavalkovich K (1996) Identification and immunolocalization of type X collagen at the ligament-bone interface. *Biochem Biophys Res Commun* 222:584–589.
5. Wei X, Messner K (1996) The postnatal development of the insertions of the medial collateral ligament in the rat knee. *Anat Embryol (Berl)* 193:53–59.
6. Messner K (1997) Postnatal development of the cruciate ligament insertions in the rat knee. morphological evaluation and immunohistochemical study of collagens types I and II. *Acta Anat* 160:261–268.
7. Petersen W, Tillmann B (1999) Structure and vascularization of the cruciate ligaments of the human knee joint. *Anat Embryol (Berl)* 200:325–334.
8. Wang IN, Mitroo S, Chen FH, Lu HH, Doty SB (2006) Age-dependent changes in matrix composition and organization at the ligament-to-bone insertion. *J Orthop Res* 24:1745–1755.
9. Woo SL, Gomez MA, Seguchi Y, Endo CM, Akeson WH (1983) Measurement of the mechanical properties of ligament substance from a bone-ligament-bone preparation. *J Orthop Res* 1:22–29.
10. Friedman MJ, *et al.* (1985) Autogenic anterior cruciate ligament (ACL) anterior reconstruction of the knee. A review. *Clin Orthop* 196:9–14.
11. Kurosaka M, Yoshiya S, Andrish JT (1987) A biomechanical comparison of different surgical techniques of graft fixation in anterior cruciate ligament reconstruction. *Am J Sports Med* 15:225–229.
12. Robertson DB, Daniel DM, Biden E (1986) Soft tissue fixation to bone. *Am J Sports Med* 14:398–403.
13. Rodeo SA, Arnoczky SP, Torzilli PA, Hidaka C, Warren RF (1993) Tendon-healing in a bone tunnel. A biomechanical and histological study in the dog. *J Bone Joint Surg Am* 75:1795–1803.
14. Woo SL, Buckwalter JA (1988) AAOS/NIH/ORS Workshop. Injury and repair of the musculoskeletal soft tissues. *J Orthop Res* 6:907–931.
15. Matyas JR, Anton MG, Shrive NG, Frank CB (1995) Stress governs tissue phenotype at the femoral insertion of the rabbit MCL. *J Biomech* 28:147–157.
16. Currey JD (1988) The effect of porosity and mineral content on the Young's modulus of elasticity of compact bone. *J Biomech* 21:131–139.
17. Ferguson VL, Bushby AJ, Boyde A (2003) Nanomechanical properties and mineral concentration in articular calcified cartilage and subchondral bone. *J Anat* 203:191–202.
18. Radhakrishnan P, Lewis NT, Mao JJ (2004) Zone-specific micromechanical properties of the extracellular matrices of growth plate cartilage. *Ann Biomed Eng* 32:284–291.
19. Noyes FR, Butler DL, Grood ES, Zernicke RF, Hefzy MS (1984) Biomechanical analysis of human ligament grafts used in knee-ligament repairs and reconstructions. *J Bone Joint Surg Am* 66:344–352.
20. Stouffer DC, Butler DL, Hosny D (1985) The relationship between crimp pattern and mechanical response of human patellar tendon-bone units. *J Biomech Eng* 107:158–165.
21. Spalazzi JP, Gallina J, Fung-Kee-Fung SD, Konofagou EE, Lu HH (2006) Elastographic imaging of strain distribution in the anterior cruciate ligament and at the ligament-bone insertions. *J Orthop Res* 24:2001–2010.
22. Wang CC, Chahine NO, Hung CT, Ateshian GA (2003) Optical determination of anisotropic material properties of bovine articular cartilage in compression. *J Biomech* 36:339–353.
23. Wang CC, Deng JM, Ateshian GA, Hung CT (2002) An automated approach for direct measurement of two-dimensional strain distributions within articular cartilage under unconfined compression. *J Biomech Eng* 124:557–567.
24. Schinagl RM, Gurskis D, Chen AC, Sah RL (1997) Depth-dependent confined compression modulus of full-thickness bovine articular cartilage. *J Orthop Res* 15:499–506.
25. Guilak F, Ratcliffe A, Mow VC (1995) Chondrocyte deformation and local tissue strain in articular cartilage: a confocal microscopy study. *J Orthop Res* 13:410–421.
26. Froimson MI, Ratcliffe A, Gardner TR, Mow VC (1997) Differences in patellofemoral joint cartilage material properties and their significance to the etiology of cartilage surface fibrillation. *Osteoarthritis Cartilage* 5:377–386.
27. Treppo S, *et al.* (2000) Comparison of biomechanical and biochemical properties of cartilage from human knee and ankle pairs. *J Orthop Res* 18:739–748.
28. Thomopoulos S, Marquez JP, Weinberger B, Birman V, Genin GM (2006) Collagen fiber orientation at the tendon to bone insertion and its influence on stress concentrations. *J Biomech* 39:1842–1851.
29. Lu HH, Jiang J (2006) Interface tissue engineering and the formulation of multiple-tissue systems. *Adv Biochem Eng Biotechnol* 102:91–111.
30. Spalazzi JP, Doty SB, Moffat KL, Levine WN, Lu HH (2006) Development of controlled matrix heterogeneity on a triphasic scaffold orthopedic interface tissue engineering. *Tissue Eng* 12:3497–3508.
31. Mikos AG, *et al.* (2006) Engineering complex tissues. *Tissue Eng* 12:3307–3339.
32. Butler DL, Goldstein SA, Guilak F (2000) Functional tissue engineering: The role of biomechanics. *J Biomech Eng* 122:570–575.
33. American Academy of Orthopaedic Surgeons (1997) *Arthroplasty and Total Joint Replacement Procedures: United States 1990 to 1997* (AAOS, Rosemont, IL).
34. Griffin LY, *et al.* (2006) Understanding and preventing noncontact anterior cruciate ligament injuries: a review of the Hunt Valley II meeting, January 2005. *Am J Sports Med* 34:1512–1532.
35. Muthupillai R, *et al.* (1995) Magnetic resonance elastography by direct visualization of propagating acoustic strain waves. *Science* 269:1854–1857.
36. Muthupillai R, Ehman RL (1996) Magnetic resonance elastography. *Nat Med* 2:601–603.
37. Lopez O, Amrami KK, Manduca A, Ehman RL (2008) Characterization of the dynamic shear properties of hyaline cartilage using high-frequency dynamic MR elastography. *Magn Reson Med* 59:356–364.
38. Lopez O, Amrami KK, Manduca A, Rossman PJ, Ehman RL (2007) Developments in dynamic MR elastography for in vitro biomechanical assessment of hyaline cartilage under high-frequency cyclical shear. *J Magn Reson Imaging* 25:310–320.